

Postbuckling behaviour of graphene-reinforced plate with interfacial effect

A. KUMAR SRIVASTAVA¹⁾, D. KUMAR²⁾

¹⁾ *Mechanical Engineering Department
Manipal University
Jaipur, India
e-mail: ashishkumar.srivastava@jaipur.manipal.edu*

²⁾ *Mechanical Engineering Department
Malaviya National Institute of Technology
Jaipur, India
e-mail: dkumar.mech@mnit.ac.in*

THE PRESENT STUDY IS AIMED TO STUDY THE POSTBUCKLING RESPONSE of the graphene sheet (GS)-reinforced plate including the effect of van-der-Waals (vdW) bonding between GS and matrix. An equivalent solid fibre (ESF) containing GS and the interfacial region is modelled, and that are randomly dispersed into the matrix with the aid of the Boolean based random sequential adsorption (RSA) technique. The elastic constants of the nanocomposite are calculated by the FEM-based homogenization procedure. It is established that interphase zone, stacking and short GSs pose the negative effect on the elastic properties of nanocomposite and postbuckling strength of the GS-reinforced plate.

Key words: graphene sheet, equivalent solid fibre, homogenization, postbuckling.

Copyright © 2018 by IPPT PAN

1. Introduction

THE TWO-DIMENSIONAL HONEYCOMB CRYSTAL LATTICE of sp^2 -hybridized carbon atoms i.e., Graphene Sheet (GS) possess extraordinary mechanical and electrical properties [1] and has been theoretically studied for seventy years [2, 3]. Even though GSs were known as an integral part of 3D materials, but it was presumed that GS does not exist in a free state and is supposed to be unstable with respect to the formation of curved structures like fullerenes and nanotubes [4]. In 2004, NOVOSELOV *et al.* [5] experimentally reported the naturally-occurring GS and attracted world-wide attention of scientists to a new window of nanoscience. The elastic modulus and tensile strength of GS are found to be nearly the same as that of the widely celebrated tube-like structure of sp^2 -hybridized carbon atoms i.e., carbon nanotube (CNT) [6]. But because of its high aspect ratio, surface

area, tensile strength, thermal and electrical conductivity associated with a low coefficient of thermal expansion and the production cost, GSs are preferred over CNTs as a reinforcing agent. With the addition of only a few percentage (by weight/volume) of GSs in soft matrix materials like polymers, the stiffness and strength of the resulting nanocomposite increase significantly [7]. GS possesses higher specific area than CNT and can interact with the matrix material at its both surfaces (i.e., upper and lower) which is higher than that of CNT (i.e., outer surface). The 2D structure of GSs has better mechanical interlocking with the polymer chains and an enlarged interfacial region at GS-matrix interface than CNTs which results in better mechanical properties of GS-reinforced nanocomposites [8, 9]. For instance, at a weight fraction of 3% of GS reinforcement, the tensile strength and Young's modulus of the high-density polyethylene (HDPE) nanocomposite is increased by about 77% and 87%, respectively, than those of the neat HDPE. In contrast, reinforcement of the same weight fraction of multi-wall CNTs (MWCNTs) in HDPE shows an increase in the tensile strength and Young's modulus of HDPE nanocomposites by 58% and 57%, respectively, as compared to the neat HDPE matrix [10].

For the reason that the GSs are of a miniature size, the proper characterization of GS-nanocomposites possessing enhanced elastic constants has been a challenging assignment either analytically or experimentally. Thus the computational simulations play a major role in the mechanical characterization of nanocomposites because of its handy nature (for different size & shape of GSs and loading pattern) as well as less computational cost and time. These computational simulations are mostly classified in two widely used simulation approaches (i) molecular and, (ii) continuum simulation. A number of publications are reported by the researchers around the world based on the molecular simulations to characterize GS-nanocomposites [11, 12]. Though molecular simulations present a better insight into the material behaviour at nanoscale but possess restrictions on small time and length scale. Whereas continuum simulations are not limited to time and length scales and are appropriate for the study of GS-reinforced nanocomposites at a comparatively less computational cost and time. Thus, the multiscale methods combining the benefits of molecular simulations at nano level and finite element methods at a macro level would be very effective to characterize the nanocomposite materials. To study the material behaviour of multiscale material like GS-reinforced nanocomposite, various literature had been reported by researchers [13–15]. In 2011, MONTAZERI and RAFII-TABAR [13] combined the molecular dynamics (MD), molecular structural mechanics (MSM), and the continuum mechanics-based finite element method (FEM) to predict the elastic properties of GS/CNT-reinforced polymer nanocomposite and reported that at low nanofiller content, GS-reinforced nanocomposites offer better elastic properties than CNT-reinforced nanocomposites. GIANNOPOULOS and KALLI-

VOKAS [14] showed that the interfacial region between GS and matrix have the positive effect on the effective elastic constants of polymer nanocomposite. GS-reinforced nanocomposites also possess higher critical buckling load than CNT-reinforced nanocomposites [15]. The simulation of an individual GS using a continuum approach, plate-like models are reported in the literature. For instance, HEMMASIZADEH *et al.* [16] presented an equivalent continuum model of a single-layered GS by integrating MD with the theory of shells. KITIPORNCHAI *et al.* [17] performed the vibration analysis of multi-layered GS using the continuum model. Analytical formulations were presented by SHOKRIEH and RAFIEE [18] to predict the elastic modulus of GS and CNT using a linkage between the molecular lattice structure and the equivalent discrete frame structure based on the nanoscale continuum mechanics approach. In order to further reduce the simulation cost, only the continuum mechanics based analysis of GS-reinforced nanocomposites (as also utilized for CNT-reinforced nanocomposites [19, 20]) was performed by KUMAR and SRIVASTAVA [21].

If no chemical bonds are available between GS and the matrix material, the GS interacts with the matrix material only by van-der-Waals (vdW) forces. This vdW interaction between embedded GS and surrounding matrix affects substantially the load transfer between the two and therefore the role of an interfacial region on the net elastic constants of GS-nanocomposite materials is substantial. Numerous studies are available in the literature on the continuum mechanics based simulation of an interfacial region. ANJOMSHOA *et al.* [22] modelled the vdW bonding between the GS and polymer matrix with a set of linear springs using the Lennard-Jones (LJ) potential with the aid of FEM whereas, NADERI and SAIDI [23] considered the same vdW interaction as a nonlinear function of the GS's deflection. Similarly, PARASHAR and MERTINY [24] employed a truss model using the FEM software ANSYS to simulate the interfacial region. The stiffness of the linear and nonlinear spring elements between CNT/GS and matrix modelled in aforementioned studies was widely computed with the concept of equivalent force, derived from an interfacial potential [15, 25]. Likewise, GEORGANTZINOS *et al.* [26, 27] have predicted Young's modulus of CNT-reinforced nanocomposite by modelling the interfacial region as spring elements. The same authors studied the elasto-plastic behaviour of CNT-reinforced rubber nanocomposites where the interfacial region was simulated via the application of special joint elements of variable stiffness which interconnect the two materials in a discrete manner [28]. The interfacial region between nano-reinforcement and matrix was also modelled as the third phase, i.e., the interphase zone having elastic properties derived from the interfacial potential [29]. A general expression for the interfacial potential, based on vdW interactions between GS and the matrix material, in terms of area and volume density of GS and the matrix respectively, was proposed by JIANG *et al.* [30], and expressions for net cohesive stresses between the GS and the ma-

trix was also derived. ZHAO *et al.* [31] extrapolated the work by JIANG *et al.* [30] and discussed the effects of spacing, size and crossing angles of the nanofillers (i.e., GS & CNT) on the effective potential of interfacial region, and reported that smaller radius CNT possess the higher cohesive energy than the large diameter CNT, and the equilibrium distance of the interphase zone enhances with the radius of CNT. Very recently, using the same cohesive zone model, SRIVASTAVA and KUMAR [32] have predicted Young's modulus and thickness of an interfacial region between matrix materials (ranging from soft to stiff) and CNT/GS.

The thickness of the interfacial region strongly affects the elastic constants nanocomposite material, especially for soft matrices [33]. The separate modelling of an interfacial region having the finite thickness from the GSs in a matrix requires the high computational cost which can be reduced by modelling a GS along with its interphase zone as an equivalent solid fibre (ESF). The assumption of the perfect bonding between ESF and the matrix material is made in a continuum model. The elastic constants of the ESF-reinforced nanocomposite material obtained by the FEM modelling should not be compared with those estimated by the micro mechanics based rule of mixtures (ROM) without considering the effect of the interphase zone. If the perfect bonding between GS and matrix is assumed, the ROM will overestimate the elastic modulus of resulting nanocomposite [34].

To impart the extraordinary elastic properties of GSs to the nanocomposite material, it is essential to resolve the issue of proper dispersion of GSs in the matrix material, since the non-uniform dispersion of GSs results in stacking and causes an adverse effect on the effective elastic constants of nanocomposites material [35]. Many researchers have devised various experimental techniques to homogeneously disperse the GSs in matrix materials [36,37]. CHEN *et al.* [36] reported a novel manufacturing method to make GS-reinforced magnesium nanocomposite by combining liquid state ultrasonic processing and solid state stirring whereas KIM *et al.* [37] utilized the melt mixing process to fabricate the GS-reinforced polyamide nanocomposite. In 2009, FANG *et al.* [38] studied the GSs reinforced polystyrene nanocomposites and having GSs diameters in two different ranges i.e., (20–40 nm) and (30–150 nm) and showed that the dispersion of GSs can also be improved by reinforcing short GSs, instead of long GSs, in the matrix material. Apart from the random dispersion of GSs into the matrix material, another important procedure to further enhance the elastic properties of the GS-reinforced nanocomposite in a specific direction is by alignment of GSs [39].

The complex geometry of actual nanocomposite possessing homogeneously dispersed GSs can be modelled by the random sequential adsorption (RSA) algorithm [40], which is widely utilized for modelling the representative volume element (RVE) of a conventional composite having randomly dispersed fibre.

The number of research articles on RSA technique is reported in the literature [41–43], but these algorithms require tedious looping calculations to predict the orientation and position of newly added non-overlapping reinforcement. In 2016, LIU *et al.* [44] reported a very efficient Boolean based RSA approach to model an RVE possessing the non-intersecting reinforcements of any shape by determining the angle and location of new reinforcement without using an iterative procedure.

Outstandingly high material constants of GSs and enhanced material constants of GS-reinforced nanocomposites further necessitates the study of plate or beam-like nanostructures made of GS-reinforced nanocomposites [45, 46]. The full load carrying capacity of these nanostructures subjected to in-plane compression and/or shear or thermal loading after buckling of the nanostructure (i.e., postbuckling behaviour) has been an area of intense study. For instance, YANG *et al.* [47] studied the postbuckling response of functionally graded (FG) GS-reinforced nanocomposite beams resting on an elastic foundation. The net material properties of each layer reinforced with randomly dispersed GSs were estimated by the micro mechanics based Halpin-Tsai model. Similarly, the postbuckling behaviour of FG GS-reinforced nanocomposite plate subjected to thermal loading was studied by SHEN *et al.* [48], wherein the elastic constants of the nanocomposite material were predicted using the same methodology as employed by YANG *et al.* [47]. It was concluded that the temperature rise, transverse shear deformation, plate aspect ratio, foundation stiffness and in-plane boundary conditions affect substantially the thermal postbuckling response of FG GS-reinforced nanocomposite plate.

It is evident from the literature that, vdW interaction between GS & matrix and the proper dispersion of GSs affects substantially the net material constants of the nanocomposite material and thus require the proper attention. It is also to be noticed that, no research article has been reported to date on the buckling and postbuckling behaviours of GS nanocomposite plate under in-plane compressive loading along with the effect of interfacial behaviour. In this study, initially the interfacial region between GS and matrix materials is modelled as a third phase and its Young's modulus and thickness are obtained by using the cohesive zone model as described in [32] and further utilized to model an equivalent solid fibre (ESF) for GS along with the corresponding third phase i.e., the interphase zone. Thereafter, ESFs are randomly dispersed or aligned in the matrix material by employing Boolean based RSA technique to make the nanocomposite RVEs. The net elastic constants of GS nanocomposite are computed with the FEM-based numerical homogenization approach. The obtained elastic constants of nanocomposite are again employed to predict the postbuckling behaviour of the GS nanocomposite plate, under in-plane compressive loading. Various studies are performed to predict the effects of bonding between GS/CNT and matrix

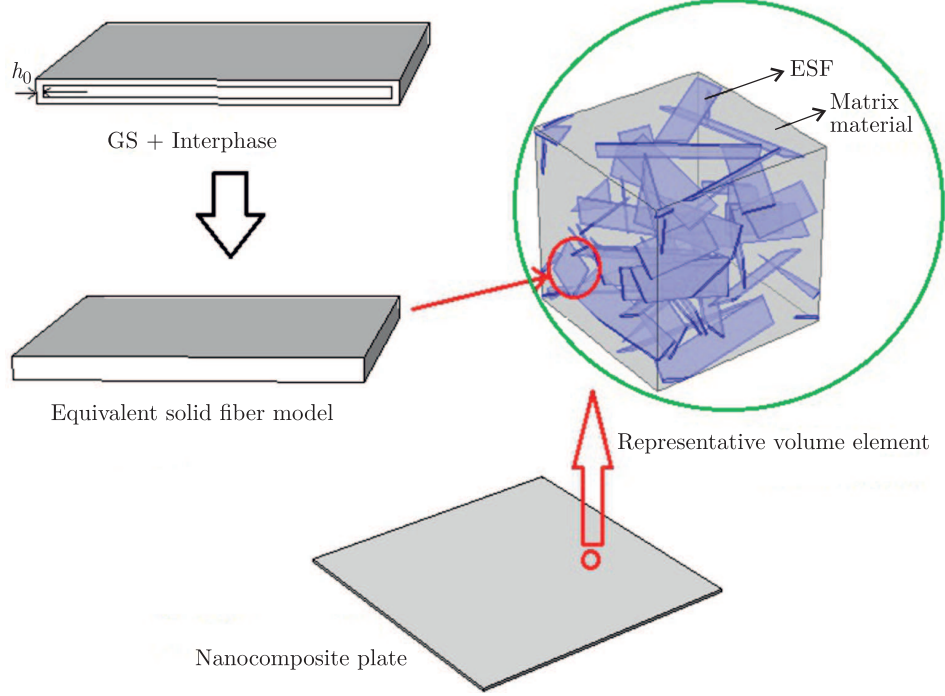


FIG. 1. Multiscale modelling procedure to form the nanocomposite plate.

materials, GS-alignment, stacking, length of GSs and geometric parameters on the postbuckling behaviour of the GS nanocomposite plate. A schematic diagram of the multiscale modelling procedure of the present problem is shown in Fig. 1.

2. Equivalent solid fiber model

The cohesive zone model (CZM) based on vdW interactions between GS and the matrix proposed by JIANG *et al.* [30] and also utilized by SRIVASTAVA and KUMAR [32, 49] in order to predict the thickness (h_0) and elastic modulus (E_I) of the hypothetical third phase i.e., the interphase zone, is employed in the present article to estimate the elastic response of equivalent solid fibre (ESF). The energy between two atoms of the distance r due to the vdW force can be represented by a pair potential. Pair potentials are the simplest inter-atomic interactions and are dependent on the distance r between two atoms. Most widely used pair potentials for simulation in chemistry, physics and engineering are Lennard–Jones (LJ) and Morse potentials. The LJ potential may be too hard to describe the repulsive force for some materials such as copper whereas Morse potentials are relatively computationally expensive [50]. JIANG *et al.* [30] have employed LJ potential to model the vdW interaction between GS and the matrix material, and obtained

cohesive energy between the matrix and GS, per unit area of GS, is given as:

$$(2.1) \quad \varphi = \frac{2\pi}{3} \rho_m \rho_c \varepsilon_I \sigma_I^3 \left(\frac{2\sigma_I^9}{15r^9} - \frac{\sigma_I^3}{r^3} \right),$$

The variation of interphase cohesive energy with respect to the inter-atomic distance r , for GS-reinforced aluminium composite, is plotted in Fig. 2. The well depth (ε_I) and vdW radius (σ_I) of the LJ potential curve for the interfacial region between GS and the matrix material can be calculated by applying the extensively used Lorentz–Berthelot (LB) mixing rule [51, 52]. The required values of different parameters employed to generate the curve are taken from [30, 50].

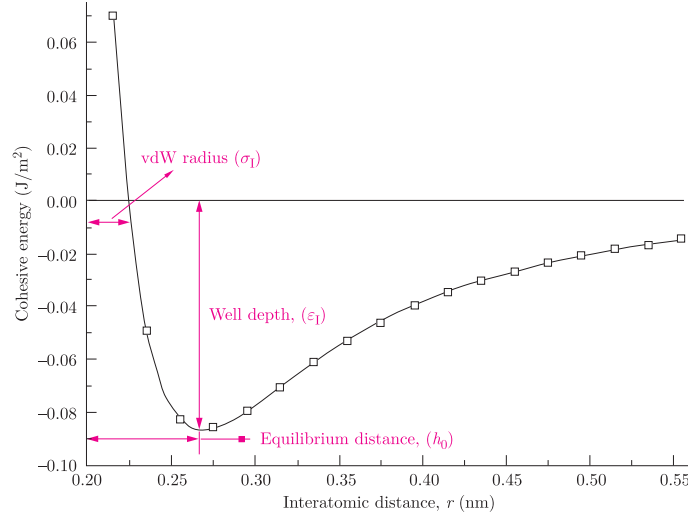


FIG. 2. Cohesive energy between GS and aluminium matrix per unit surface area of GS.

The detailed explanation of this approach to find the thickness (h_0) and Young's modulus (E_I) of this third phase are given in [32], and for ready reference given below.

The equilibrium distance (i.e., h_0) between the GS and matrix by satisfying, $\partial\varphi/\partial r = 0$:

$$(2.2) \quad h_0 = 0.8584\sigma_I.$$

The Young's modulus of the interphase zone (i.e., E_I) for the equilibrium position (at $r = h_0$), is computed by:

$$(2.3) \quad E = \frac{\partial^2 \varphi}{\partial^2 S},$$

where, strain (S) at any distance is taken as, $S = r - h_0/h_0$ and obtained the expression for Young's modulus is given by:

$$(2.4) \quad E_I = 8\pi h_0 \rho_m \rho_c \varepsilon_I \sigma_I^2 \left(\frac{\sigma_I^{10}}{r^{11}} - \frac{\sigma_I^4}{r^5} \right),$$

where r represents the distance between GS & matrix material, and the area (ρ_C) and the volume density (ρ_m) specify the number of carbon atoms per unit surface area of GS and number of atoms per unit matrix volume, respectively.

After obtaining Young's modulus (E_I) and the thickness (h_0) of the interphase zone, the plate-like continuum structure of GS and the corresponding interphase zone is replaced by an equivalent solid fibre (ESF) and utilized to form an RVE consisting of uniformly distributed ESFs as shown in Fig. 1. Where the position and orientation of each ESF are obtained by employing uniform random numbers as discussed in Section 3. To model the ESF for GS and the interphase zone, the nanofiller and corresponding interphase region have to be transformed to ESF in accordance with the micromechanics approach. The perfect bonding is assumed between GS and the interphase zone. Thus the same axial force is applied to GS & corresponding interphase region and ESF to obtain the effective width & thickness of ESF by equaling axial deformation of GS & interphase zone and ESF.

Therefore, the axial force applied on the ESF is given as:

$$(2.5) \quad F_{ESF} = F_{GS} + F_{INT},$$

where F_{GS} and F_{INT} are the fractions of the applied force (i.e., F_{ESF}) borne by GS and the interphase region, respectively.

Similarly, the same axial deformation of GS, the interphase zone and ESF can be represented as

$$(2.6) \quad \Delta L_{GS} = \Delta L_{INT} = \Delta L_{ESF},$$

where ΔL represents the change in longitudinal length.

While estimating the width and thickness of newly formed ESF, it is supposed that the change in width/thickness of GS is constant (i.e., κ) and therefore, Eqs. (2.5) and (2.6) reduces to:

$$(2.7) \quad E_{ESF}(w + 2\kappa)(t + 2\kappa) = E_{GS}wt + E_{INT}[(w + 2h_0)(t + 2h_0) - wt],$$

where w and t are the width and thickness of GS, respectively; κ represents the increase in width/thickness of GS while modelling the ESF.

To predict the width/thickness of isotropic ESF using Eq. (2.7), it is necessary to have the value of Young's modulus of ESF. The Young's modulus of ESF (i.e., E_{ESF}) can be computed by using micro-mechanical schemes like ROM, The Halpin-Tsai method and composite cylinder assemblage (CCA) models etc. Out of which ROM and the Halpin-Tsai method are simple, accurate and yield

the same expressions for Young's modulus and Poisson's ratio aligned fiber reinforced composites [53]. The corresponding expression for Young's modulus and Poisson's ratio of ESF are given as:

$$(2.8) \quad E_{ESF} = V_{GS}E_{GS} + (1 - V_{GS})E_{INT}.$$

Similarly, the Poisson's ratio of ESFs can also be evaluated with the aid of ROM and given as:

$$(2.9) \quad \nu_{ESF} = V_{GS}\nu_{GS} + (1 - V_{GS})\nu_{INT}$$

Where V_{GS} stands for the volume fraction of GS in ESF and computed by

$$(2.10) \quad V_{GS} = \frac{(wt)}{(w + 2h_0)(t + 2h_0)}$$

3. Modeling and characterization of ESF-reinforced RVE

To estimate the effective elastic constants of the GS-reinforced nanocomposite, an RVE is created consisting of ESFs reinforced in a matrix material using the Boolean-based RSA technique as also employed by SRIVASTAVA and KUMAR [54] for CNT-reinforced nanocomposites. ESF is described by its origin O and Euler angles θ and φ in the xyz coordinate system, as shown in Fig. 3. In the Boolean based RSA approach (described in Fig. 4), initially the first reinforcement is placed randomly (i.e., random-orientation and -position) into the RVE volume, and then new reinforcement is considered for adsorption in RVE volume only if it does not intersect with the previously adsorbed reinforcements. A new ESF is

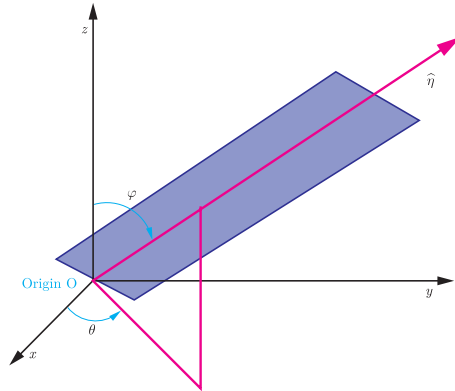


FIG. 3. Coordinate system and definitions of θ and ϕ for an ESF (consisting of GS and corresponding interphase zone).

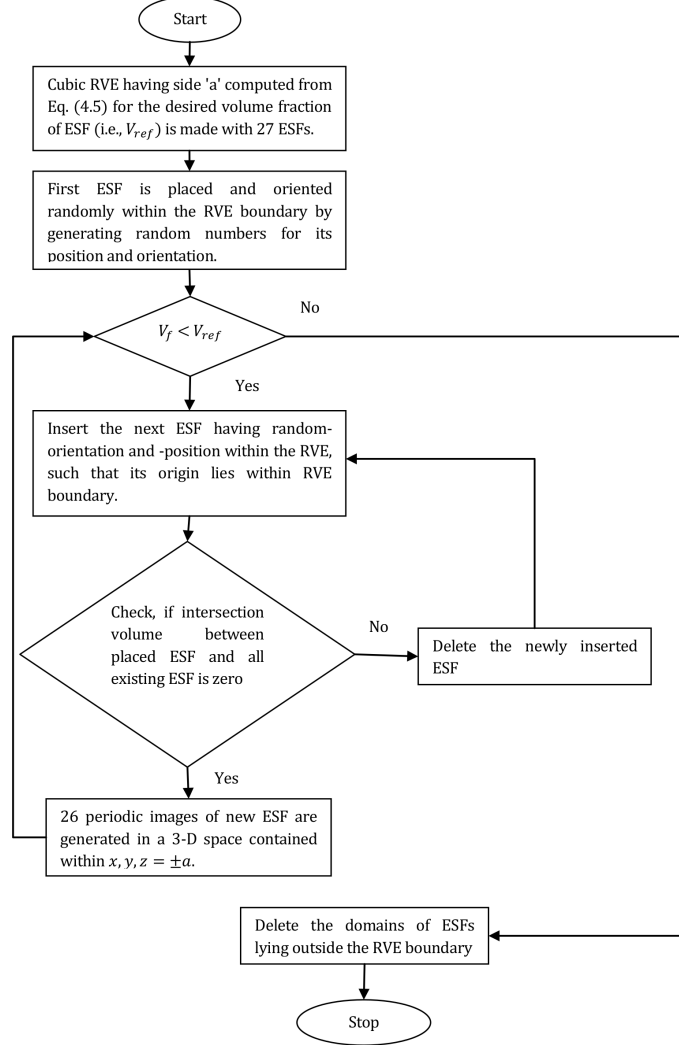


FIG. 4. Boolean based RSA algorithm to generate periodic RVE.

kept on adding into the RVE till the volume fraction of ESF (i.e., V_f) reaches to the reference volume fraction (i.e., V_{ref}), and when the reference volume fraction is reached, the parts of ESFs lying outside the RVE boundary are chopped off to form the resulting RVE. The total number of ESFs is limited to 27 in the present study. Using the Boolean based RSA algorithm, the non-intersecting, randomly-oriented and -positioned ESFs-reinforced RVE is modelled as shown in Fig. 5a. The same methodology is also employed to RVEs with randomly-positioned, but aligned ESF, to study the effect of GS-alignment on the elastic constants of the nanocomposite, as shown in Fig. 5b. Similarly, to study the effect of stacking of

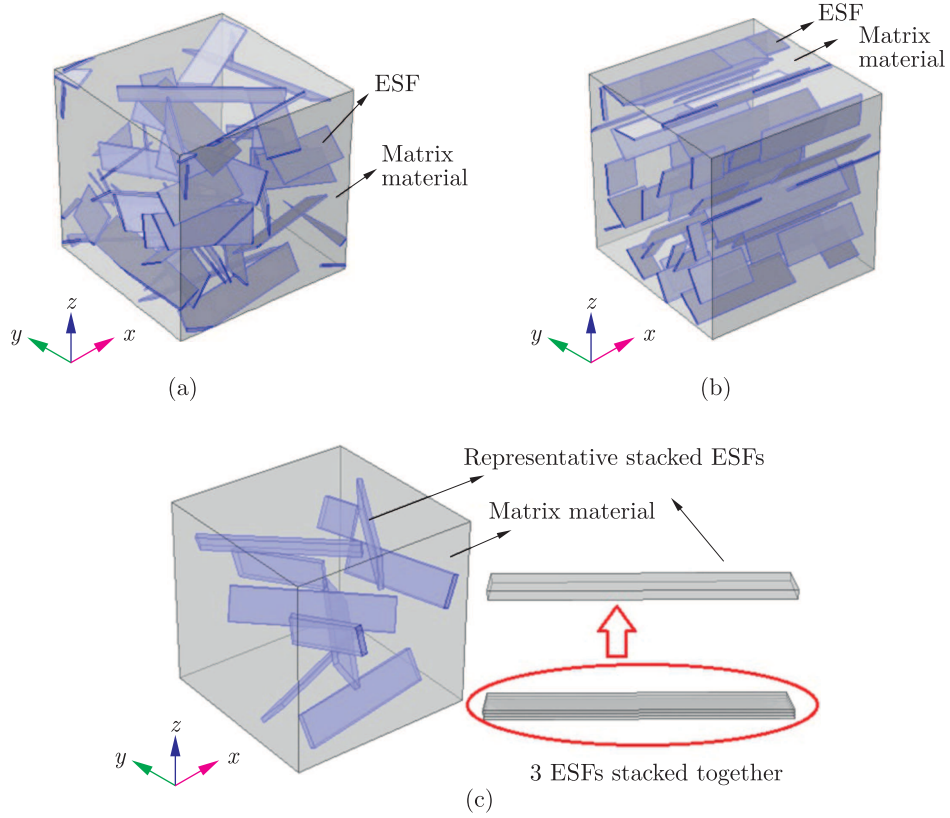


FIG. 5. Periodic RVE containing: a) randomly-oriented and -positioned ESFs, b) aligned and randomly-positioned ESFs, c) randomly-oriented and -positioned stacked ESFs.

GSs on elastic constants of the resulting nanocomposite material, three GSs are stacked together and randomly-oriented and -positioned in the matrix volume as shown in Fig. 5c. Modeled heterogeneous RVEs (consisting of GS and the matrix material) are subjected to periodic boundary conditions and the homogenization approach in order to estimate the homogeneous elastic properties of resulting nanocomposite [32].

4. Micromechanics based Halpin–Tsai model

The widely used Halpin-Tsai model to evaluate the elastic properties of fibre composites is also employed with modifications by different authors to predict the elastic properties of GS-reinforced nanocomposites [48, 55]. To model the elastic modulus of the GS-reinforced nanocomposites, it was assumed that ESFs of GSs act as an effective rectangular solid fibre with the width (w_{ESF}), length (L_{ESF}),

and thickness (t_{ESF}). The modified Halpin–Tsai equations for GS-reinforced nanocomposites are given as:

$$(4.1) \quad E_C = E_m \left(\frac{3}{8} \frac{1 + \xi \eta_L V_f}{1 - \eta_L V_f} + \frac{5}{8} \frac{1 + 2\eta_w V_f}{1 - \eta_w V_f} \right),$$

where

$$(4.2) \quad \eta_L = \frac{(E_{ESF}/E_m) - 1}{(E_{ESF}/E_m) + \xi},$$

$$(4.3) \quad \eta_w = \frac{(E_{ESF}/E_m) - 1}{(E_{ESF}/E_m) + 2}.$$

E_C represents the elastic modulus of the GS-reinforced nanocomposite, E_{ESF} and E_m are the ESF and matrix moduli. For rectangular reinforcements GSs, the parameter ξ is given as

$$(4.4) \quad \xi = 2 \left(\frac{(w_{ESF} + L_{ESF})/2}{t_{ESF}} \right),$$

where w_{ESF} , L_{ESF} and t_{ESF} represent the width, length, and thickness of ESF. For the axial modulus, the Halpin–Tsai equation reduces to ROM [53]. The volume fraction V_f of the reinforcement in the RVE is calculated using

$$(4.5) \quad V_f = \frac{V_{ESF}}{V_{RVE}} = \frac{w_{ESF} L_{ESF} t_{ESF}}{(a^3 - n w_{ESF} L_{ESF} t_{ESF})}.$$

5. FEM procedure for postbuckling analysis of GS nanocomposite plate

For the postbuckling analysis of the GS-reinforced nanocomposite plate, the FEM-based commercial code ANSYS is employed and the eight-node shell element (i.e., SHELL281) with 6 degrees of freedom (i.e., 3-translational and 3-rotational) in a plane stress state is used to discretize the GS-nanocomposite plate. The resulting set of nonlinear algebraic equations are solved by employing the arc-length method. A complete formulation for the postbuckling analysis is provided by KUBIAK [56], for the sake of ready reference a brief description of the procedure is given below.

It is a well-established fact that studies involving the buckling and postbuckling analysis of thin plate-like structures under in-plane compressive loads need some kind of imperfections in terms of out-of-plane displacement (provided either by a little transverse force or by specifying a small initial displacements) to initiate the buckling response. Therefore, in the present study, the buckling

and postbuckling analysis of the GS ESF-reinforced nanocomposite plate is performed in two stages: (1) the eigenvalue linear buckling analysis, and (2) the nonlinear (geometric) postbuckling analysis. In the eigenvalue buckling analysis, the buckling load and corresponding the buckling mode are evaluated, and thereafter, the buckled mode shape is further employed to provide an initial tiny perturbation/imperfection into the GS ESF-reinforced nanocomposite plate. Subsequently, the nonlinear postbuckling analysis of the GS ESF-reinforced nanocomposite plate using FEM is performed by utilizing an iterative procedure wherein the in-plane compressive load on the ESF-reinforced nanocomposite plate is increased gradually in each successive step, and the corresponding out-of-plane deformation is obtained.

The nonlinear algebraic equations of a discrete system are given by:

$$(5.1) \quad [\bar{\mathbf{K}}(\mathbf{u})]\{\mathbf{u}\} - \{\mathbf{P}\} = 0,$$

where $[\bar{\mathbf{K}}]$ is the tangent stiffness matrix depending on the nodal displacement $\{\mathbf{u}\}$, and the net nodal force vector $\{\mathbf{P}\}$.

At a particular load step, Eq. (5.1) for the i th iteration can be rewritten as:

$$(5.2) \quad [\bar{\mathbf{K}}_i]\{\Delta\mathbf{u}_i\} = \{\Delta\mathbf{P}_i\},$$

where the increment of displacement (i.e., $\Delta\mathbf{u}_i$) is assumed to comply with the following expression:

$$(5.3) \quad \{\mathbf{u}_{i+1}\} = \{\mathbf{u}_i\} + \{\Delta\mathbf{u}_i\},$$

and

$$\{\Delta\mathbf{P}_i\} = \zeta\{\mathbf{P}^a\} - \{\mathbf{P}_i^r\},$$

wherein $\{\mathbf{P}^a\}$ represents the applied nodal force vector adjusted via the load factor ζ ($-1 < \zeta < 1$) in the subsequent iterative process and $\{\mathbf{P}_i^r\}$ is the restoring forces vector for the i th iteration.

Therefore, the Eq. (5.2) in the incremental form of any intermediary step (i.e., at the substep n and the iteration i) has the following form:

$$(5.4) \quad [\bar{\mathbf{K}}_i]\{\Delta\mathbf{u}_i\} - \Delta\zeta\{\mathbf{P}^a\} = (\zeta_n + \zeta_i)\{\mathbf{P}^a\} - \{\mathbf{P}_i^r\}.$$

The incremental load factor (i.e., $\Delta\zeta$) is evaluated by the arc-length (l_i) for the i th iteration, as reported by FORDE and STIEMER [57], and given as:

$$(5.5) \quad l_i^2 = \Delta\zeta_i^2 + \beta^2\{\Delta\mathbf{u}_n\}^T\{\Delta\mathbf{u}_n\},$$

where, β represents the scaling factor and $\Delta\mathbf{u}_n$ is the sum of all the displacement increments $\Delta\mathbf{u}_i$ up to i th iteration of the current load step.

The convergence for each iteration process is checked by the following error tolerance procedure:

$$(5.6) \quad \|\mathbf{R}\| \leq \alpha \|\Delta \mathbf{P}\|,$$

where \mathbf{R} refers to the residual force at each iteration (i.e., $[\bar{\mathbf{K}}_i]\{\Delta \mathbf{u}_i\} - \{\Delta \mathbf{P}_i\}$) and α is a tolerance parameter which is chosen as 10^{-4} .

FEM based software ANSYS is used to carry out the buckling and post-buckling study of the GS ESF-reinforced nanocomposite plate through a macro written in APDL (i.e., ANSYS Parametric Design Language).

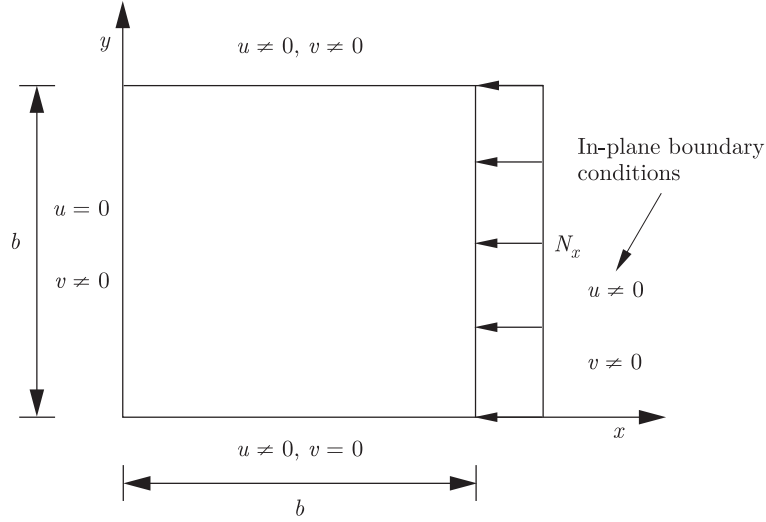


FIG. 6. In-plane boundary conditions for a square plate subjected to uni-axial compression load applied on $x = b$ edge.

To perform the buckling and postbuckling studies of the GS nanocomposite plate all edges simply supported (i.e., SSSS) the boundary condition is employed. The in-plane boundary conditions on edges $x = 0$, $x = b$, $y = 0$ and $y = b$ related to in-plane displacements in x - and y - directions (i.e., u and v , respectively) are depicted in Fig. 6. The axial compression load per unit width is applied on the edge $x = b$ for uni-axial loading, and on the edges $x = b$ and $y = b$ for bi-axial loading.

6. Present study

In this study, initially, an ESF is formed to represent a GS along with the interphase zone for different matrix materials. The isotropic effective material constants of the heterogeneous nanocomposite material are estimated by the proper

application of periodic boundary conditions on an RVE generated through RSA technique. The obtained material constants of ESFs-reinforced nanocomposite are presented and discussed in Section 7.2. The material constants of GS and the geometric dimensions are given below:

Young modulus $E_f = 1$ TPa, Poisson's ratio $\nu = 0.3$.

Length $L_{GS} = 100$ nm, width ' w ' of GS is computed by opening a cylindrical shaped CNT into a plate-like structure using the following relation:

$$(6.1) \quad w = \frac{\pi(r_0^2 - r_i^2)}{r_0 - r_i}$$

where the outer radius of CNT, r_0 is equal to 3.6 nm and inner radius of CNT, r_i is equal to 3.2 nm. The thickness of GS, i.e., $t = r_0 - r_i$.

Thereafter, the effective material constants of the GS-reinforced nanocomposite material are further utilized to study the buckling and postbuckling behaviour of the GS-reinforced nanocomposite plate. The square nanocomposite plate having a width-to-thickness ratio equal to 50 is utilized in the current study to predict the postbuckling behaviour of the GS-reinforced nanocomposite plate under different boundary and loading conditions. The effects of various parameters, viz. perfect and imperfect bonding, ESF-alignment, ESF-stacking, length of ESF, matrix materials and geometric parameters (i.e., the aspect ratio and the width-to-thickness ratio of the plate) on the buckling and postbuckling response of GS-reinforced nanocomposite plates, are studied and discussed in Section 8.2.

7. Elastic constants of GS-reinforced nanocomposites

7.1. Validation

To verify the procedure followed in the current study to characterize the GS-reinforced nanocomposite material, an ESF-reinforced nanocomposite system is considered and its effective elastic modulus obtained through FEM based software COMSOL Multiphysics are compared with the value obtained through the semi-empirical Halpin–Tsai equation as discussed in Section 4 and given by Eq. (4.1) and also with the results reported in literature.

Initially, the interphase zone between GS and the different matrix material is characterized in terms of its Young's modulus and thickness (i.e., the equilibrium distance, h_0) [32] for GS-reinforced nanocomposites. The obtained values of Young's modulus of the hypothetical material of the interphase zone and the corresponding thickness for different matrix materials (i.e., polyethylene (PE), magnesium (Mg), copper (Cu), Iron (Fe), Aluminum (Al) and Gold (Au)) (directly taken from reference [32]) are employed to model and characterize an ESF for its elastic modulus (i.e., E_{ESF}) and change in width/thickness of GS

(i.e., κ) by following the procedure mentioned in Section 2. The Poisson's ratios of different interphase zones are taken as 0.3. The obtained values of E_{ESF} and κ of ESF are given in Table 1. Thus the width and thickness of newly formed ESF for GS along with interphase zone are $w_{ESF} = (w + 2\kappa)$ and $t_{ESF} = (t + 2\kappa)$ respectively as also used in Eq. (2.7).

Table 1. Young's modulus of ESF and change in width/thickness of GSs for different matrix material.

Matrix material [Young's modulus of matrix in GPa]	Modulus of interphase zone [GPa] [32]	Thickness of interphase zone [nm], h_0 [32]	Young's modulus of ESF [GPa] (E_{ESF})	Change in width/thickness of GS (κ) [nm]
PE [3.4]	8.9658	0.3283	369.4078	0.3331
Mg [45]	3.1885	0.2755	436.5826	0.2496
Iron [211]	6.6420	0.3243	503.1041	0.1948
Cu [130]	9.3378	0.2469	510.5524	0.1895
Al [70]	8.6854	0.2689	456.9322	0.2336
Au [78]	16.5792	0.2268	501.0694	0.1995

Thereafter, ESFs are randomly-positioned and -oriented into the matrix material to form an RVE using the Boolean based RSA technique to characterize the GS-reinforced nanocomposites for its Young's modulus. The RVE is subjected to periodic boundary conditions. The obtained value of the elastic modulus of the nanocomposite is matched in Table 2 with the value obtained from the semi-empirical Halpin-Tsai method and with the results reported in the literature. Using the FEM-based procedure, the net elastic modulus of nanocomposite material is computed as an average of nearly isotropic elastic moduli of RVE obtained in x , y and z directions (i.e., $E = (E_x + E_y + E_z)/3$). It can be observed

Table 2. Comparison of Young's modulus (in GPa) of the nanocomposite.

Matrix material	FEM [Present study]	Halpin-Tsai model [Eq. (4.1)]	Reference		Deviation between FEM and reference results (%)
			Experimental	Molecular Dynamics (MD)	
PE	1.6683	1.6792	1.5660 [59]	–	6.1319
Mg	13.7145	13.7869	14.6000 [60]	–	6.4567
Iron	203.0791	203.5862	214.1000 [61]	–	5.4269
Cu	96.2685	96.3156	104.0000 [62]	–	8.0311
Al	66.0425	66.1133	67.0000 [63]	–	1.4498
Au	116.5893	116.7410	–	118.5800* [64]	1.7074

*Taken as the average of Young's moduli of armchair and zigzag GS-reinforced Au nanocomposite.

from Table 2 that FEM based results are in good agreement with the results obtained from Halpin–Tsai and reported in reference as well.

A comparative study between the computational time taken by the the FEM based proposed 2-phase model (i.e., ESF-reinforced Al nanocomposite), 3-phase model (i.e., GS-reinforced Al nanocomposite with the interphase zone) and the widely employed molecular dynamics (MD) is also reported in Table 3. Aluminium is taken as a matrix material and volume of RVE is taken kept as $50.5 \times 50.5 \times 50 \text{ \AA}$ in x -, y - and z -direction, respectively. To perform the MD simulation, open source code LAMMPS (Large-scale Atomic/Molecular Massively Parallel Simulator) [65] distributed by Sandia national laboratories is used in the present study. The inter-atomic potential that acts in between the covalently bonded carbon atoms of the GS is computed using the AIREBO (Adaptive Inter-molecular Reactive Empirical Bond Order) potential function. Whereas, widely used Embedded Atom Method (EAM) is employed to model the pair-wise interactions between aluminium (Al) atoms by the application of EAM/ALLOY potential, which can be used to describe the interaction between metals and metal alloy. The long-range Lennard–Jones 12-6 potential as given in Eq. (7.1), is further deployed to account for the non-bonded interactions between GS and Al matrix.

$$(7.1) \quad E = 4\varepsilon \left[\left(\frac{\sigma}{r} \right)^{12} - \left(\frac{\sigma}{r} \right)^6 \right], \quad r < r_c,$$

where r_c is the LJ cutoff radius after which the vdW interaction is very weak and can be neglected and is chosen as 2.5σ (i.e., 7.83125 \AA). The parameters ε and σ are the coefficients of the well depth energy and equilibrium distance, respectively. These parameters for the interactions between carbon atoms and Al atoms are computed applying widely used Lorentz Berthelot (LB) rules [52] and given as $\sigma = 3.1325 \text{ \AA}$ and $\varepsilon = 0.003457 \text{ eV}$. The used parameters of Al and C atoms are listed in Table 3.

Table 3. 3 LJ pair potential parameters for C and Al atoms.

LJ Potential parameters	Carbon, C	Aluminum, Al
σ (\AA)	3.41500	2.8500
ε (eV)	0.00239	0.0050

For the MD simulation, the GS of dimension $50.5 \times 50.5 \text{ \AA}$ is selected. The periodic boundary condition is applied in all the three directions, and the RVE is given constant strain in the armchair and zigzag direction, respectively to predict the stress-strain behaviour of the nanocomposite. The GS is spanned through the total length of the unit cell. The equilibrated molecular structure

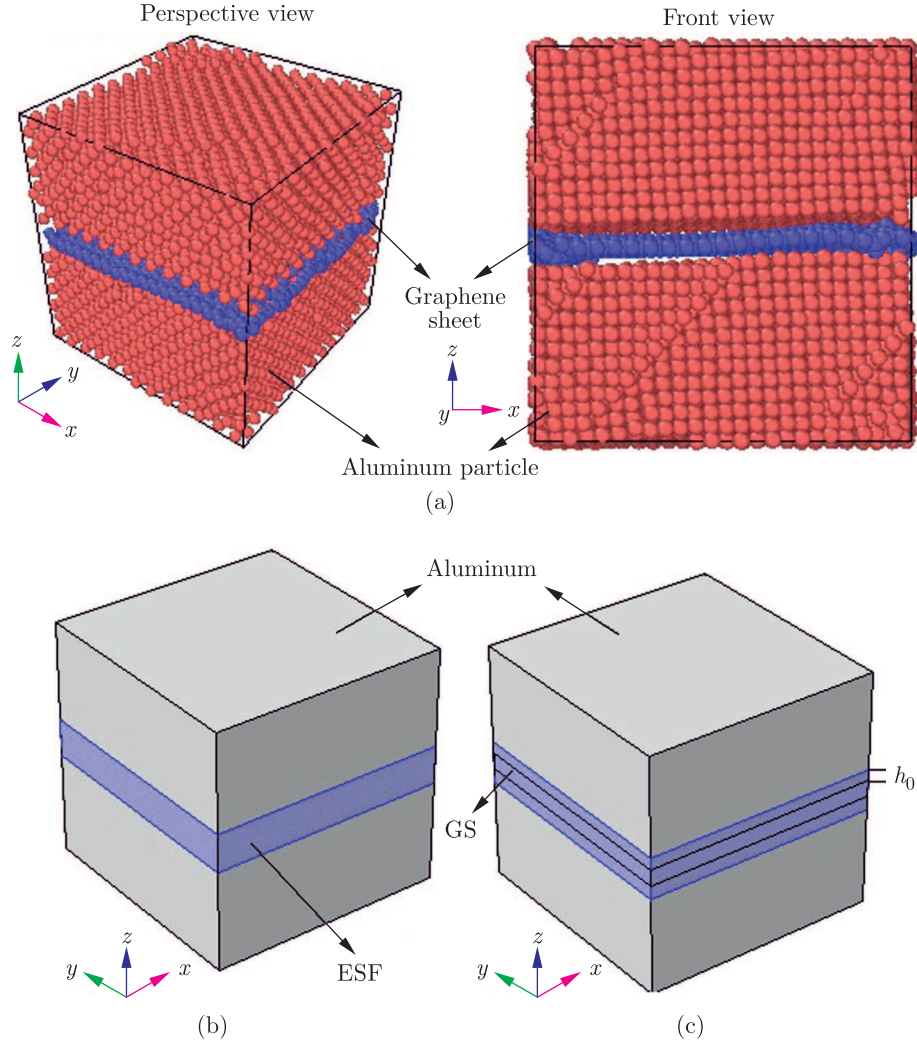


FIG. 7. a) MD simulation based equilibrated GS reinforced Al nanocomposite RVE; b) Two-phase model of FEM based RVE (i.e., ESF reinforced Al nanocomposite); and c) Three-phase model of FEM based RVE (i.e., GS reinforced Al nanocomposite with interphase zone).

(Fig. 7a) with minimized energy is accomplished by performing the sequence of energy minimization, NVT and NPT ensembles. It is noted that NVT ensemble stands for the volume and temperature being fixed during the simulation and NPT ensemble stands for the pressure and temperature being fixed during the simulation. All simulation is carried out at 300 K. After the equilibration process, the dimension of RVE becomes $50.8 \times 50.6 \times 53.7 \text{ \AA}$ and the volume fraction of GS-reinforcement is 6.8912%. MD simulation is carried under NVT

conditions by applying a constant strain rate on the RVE. MD simulation runs for 200,000 steps and the time step is taken as 0.5 fs. Results are obtained by using a personal computer equipped with the processor AMD A8-5550M APU with installed RAM of 8 GB. The obtained stress-strain behaviour of the nanocomposite is given in Fig. 8 and the corresponding computational times have also been tabulated in Table 4.

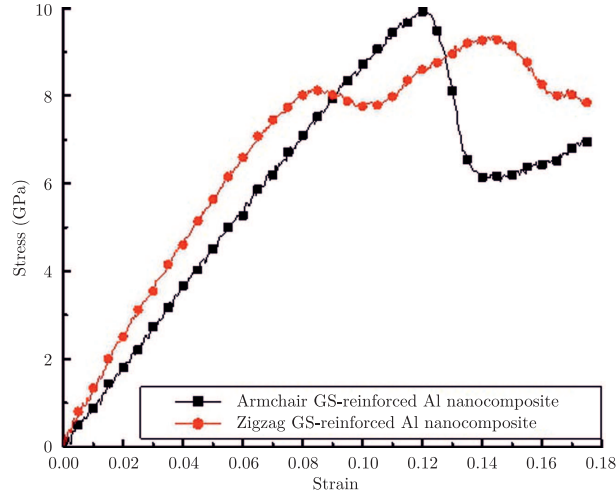


FIG. 8. Stress-strain behaviour of GS-reinforced Al nanocomposite ($v_f = 6.8912\%$).

It can be observed from the Table 4 that, the FEM-based simulations are far more computationally effective in comparison with MD based simulations. The results obtained in the armchair and zigzag direction are averaged as taken by [66] to compare with the results obtained by the FEM based continuum model having material isotropy as also reported by [67]. While comparing the 2- and 3-phase FEM based models, 3-phase models are slightly more computationally expensive than 2-phase models which will enhance substantially by increasing the number of GSs in RVE with almost the same accuracy of results.

Table 4. Comparison of Young’s modulus for Al GS aligned nanocomposite.

Molecular Dynamics					FEM		Difference
Armchair	Simulation time [Hour]	Zigzag	Simulation time [Hour]	Average	FEM	Simulation time [Hour]	
120.9374	2:08:08	89.6547	2:05:25	105.2961	107.1548 (2 phase model)	0:00:52	1.7344 %
					107.1543 (3 phase model)	0:00:57	1.7341 %

It is to mention here that the FEM-based 2-phase procedure is employed in Section 6.2 of the current study to predict the other elastic constants of GS-reinforced nanocomposite materials.

7.2. Effective material constants of GS nanocomposite

In this section, stiffness properties of GS-reinforced nanocomposites are estimated, for 3% volume fraction of GS-reinforcement using FEM. Initially, the ESF-reinforced nanocomposite RVE is modelled by the Boolean-based RSA technique. Thereafter, the stiffness properties of different nanocomposites are obtained through the homogenization technique and listed in Table 5. From Table 5, it can be observed that the values of estimated Young's and shear moduli of various nanocomposites depict good isotropy because of the random-orientation of GSs, irrespective of the types of the matrix material. It is also clear from the Table 5 that the GSs are found to be a better reinforcing element in soft polymers (like PE) as compared to stiff materials (like Iron). For instance, in the case of PE matrix reinforced with 3% volume fraction of uniformly-oriented and -positioned GSs, the enhancement in Young's modulus of the matrix is approximately 47.9% whereas, for Iron matrix, the enhancement obtained is 2.9%. To study the effect of alignment and stacking of GS (as shown in Figs. 5b and 5c) on the elastic constants of the nanocomposite material, The GS-PE nanocomposite is modelled and corresponding stiffness properties are shown in Table 6. The effect of length of GSs on the elastic properties of the nanocomposite material is also studied and given in Table 6 for the RVE having GSs of length 50 nm (i.e., half of the length taken from other parametric studies) as also considered in literature for CNT-reinforced RVE [68, 69].

Table 5. Stiffness properties of nanocomposite having 3% of uniformly-oriented and -positioned GSs.

Matrix material [Elastic modulus of matrix in GPa]	Stiffness Properties [GPa]								
	E_x	E_y	E_z	G_{xy}	G_{xz}	G_{yz}	ν_{xy}	ν_{xz}	ν_{yz}
PE [3.4]	5.1563	5.7441	4.1873	2.0681	1.6368	1.7330	0.2661	0.2989	0.2909
Mg [45]	50.2856	51.0145	49.1384	19.4700	19.1085	19.3898	0.2929	0.2984	0.3012
Iron [211]	217.1221	217.4442	216.6902	83.5973	83.4081	83.6791	0.2991	0.2996	0.3002
Cu [130]	136.7623	137.3047	135.9715	52.7182	52.3487	52.7689	0.2977	0.2992	0.3005
Al [70]	75.9084	76.5568	74.8685	29.2911	28.9237	29.3679	0.2955	0.2988	0.3009
Au [78]	84.5267	85.2332	83.4128	32.6261	32.2246	32.7195	0.2956	0.2987	0.3009

In order to make a comparison between the stiffness properties of GS- and CNT-reinforced plates, CNT-reinforced nanocomposites are also characterized with and without the interphase zone. ESFs are modelled for CNT reinforced

Table 6. Effect of different parameters on the stiffness properties of PE-nanocomposite having 3% of GS.

Parameter	Stiffness Properties [GPa]								
	E_x	E_y	E_z	G_{xy}	G_{xz}	G_{yz}	ν_{xy}	ν_{xz}	ν_{yz}
Alignment of GS (x -direction)	9.2656	4.1102	3.9104	1.9017	1.6590	1.5402	0.2899	0.1413	0.3610
Stacked GS	4.1492	4.2583	3.9401	1.8673	1.4974	1.5744	0.3236	0.2771	0.2766
Short GS	4.7251	4.9890	4.2052	1.9956	1.6436	1.8299	0.2703	0.2991	0.2945

Table 7. Elastic modulus and radius of CNT-ESF reinforced in PE matrix.

Type of bonding	$E_{CNT-ESF}$ [GPa]	$r_{CNT-ESF}$ [nm]
Imperfect	525.5178	2.2843
Perfect	1000.0000	1.6492

Table 8. Stiffness properties of CNT/GS-reinforced PE-nanocomposites ($V_f = 0.03$).

Nanofiller	Type of bonding	Stiffness Properties [GPa]								
		E_x	E_y	E_z	G_{xy}	G_{xz}	G_{yz}	ν_{xy}	ν_{xz}	ν_{yz}
CNT	Perfect	4.3915	4.6175	5.8612	2.0848	1.7963	1.8462	0.3149	0.2495	0.2343
	Imperfect	4.0690	4.0953	4.9392	1.5514	1.7055	1.5910	0.3148	0.2630	0.2527
GS	Perfect	5.7405	7.0541	5.0198	2.6985	2.2018	2.3623	0.2264	0.2980	0.2923
	Imperfect	5.1563	5.7441	4.1873	2.0681	1.6368	1.7330	0.2661	0.2989	0.2909

in PE matrix using the same procedure as discussed in Section 2. The obtained values of Young’s modulus and radius of CNT-ESF for perfect and imperfect bonding between CNT and matrix material are given in Table 7. Thereafter, the stiffness properties of CNT- and GS-reinforced PE nanocomposites are compared in Table 8. It can be seen from Table 8 that, GSs are better reinforcing nanofiller than CNTs for both type of bonding (i.e., perfect and imperfect). It is also found that the interfacial effect leads to a reduction in the elastic properties of PE-nanocomposite for both nanofillers.

8. Postbuckling study

8.1. Validation

To verify the accuracy and validity of the approach to study the buckling and postbuckling responses of the GS-reinforced nanocomposite plate, the results predicted from the nonlinear FEM analysis with the aid of ANSYS is equalled with the results reported in the literature. All edges simply-supported (i.e., SSSS)

the isotropic square plate subjected to edge uni-axial compression is taken for comparing its buckling and postbuckling responses with that presented by SUNDARESAN *et al.* [70]. SUNDARESAN *et al.* [70] have utilized the FEM based on the 8-node isoparametric plate element with 5 degrees of freedom per node to predict the postbuckling response of the plate whereas, in this study SHELL281 element possessing 6 degrees of freedom is employed. The material properties (i.e., elastic modulus = 3×10^6 Psi, and Poisson's ratio is 0.25) and the width-to-thickness ratio (i.e., $b/h = 50$) taken for the comparison purpose are similar to those utilized by SUNDARESAN *et al.* [70].

While comparing, the results, the applied uni-axial edge compressive load N_x and the corresponding maximum transverse deflection of the plate w_{max} , are normalized as follows

$$(8.1) \quad \lambda = \frac{N_x b^2}{\pi^2 D} \quad \text{and} \quad W^* = \frac{w_{max}}{h},$$

where D , the flexural rigidity of plate, is given by $\frac{Eh^3}{12(1-\nu^2)}$; b is the side of the square plate, and; h represents the thickness of the plate.

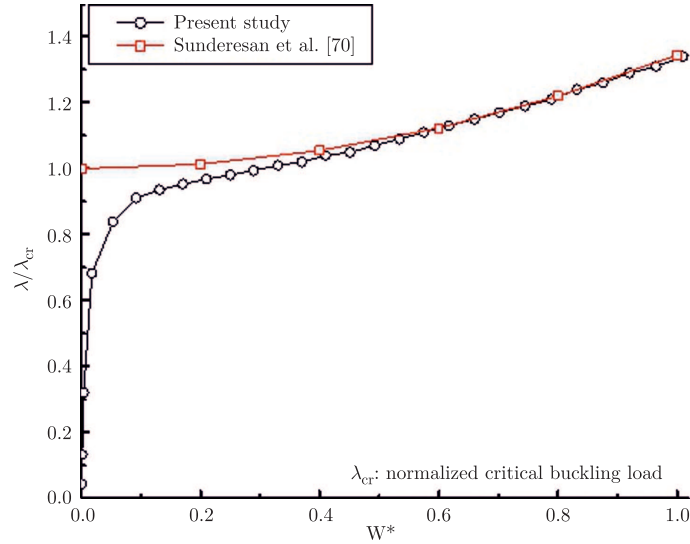


FIG. 9. Validation of postbuckling response of SSSS isotropic plate subjected to uni-axial compression.

As shown in Fig. 9, the postbuckling response and the critical buckling load obtained using the present methodology is in good agreement with that of [70]. Little deviation in the plots in Fig. 9 can be attributed to the different type of elements used in [70] and the present study, as also commented by LE-MANH and LEE [71].

8.2. Postbuckling response of GS-reinforced nanocomposite plate

After the validation of the postbuckling approach, the buckling and postbuckling behaviour of the GS-reinforced nanocomposite plate, subjected to in-plane compressive load is presented and results are discussed. The effective elastic constants of GS/ESF nanocomposite obtained in the previous section are utilized to study the effects of perfect and imperfect bonding, ESF-alignment and geometric parameters (i.e., the aspect ratio and width-to-thickness ratio) on buckling and postbuckling responses of GS-ESF-reinforced nanocomposite plates. Excluding the study on the effect of the matrix material on the postbuckling behaviour of the GS-nanocomposite plate, all other studies are conducted for ESF-reinforced PE nanocomposite plate. Similarly, except the study on the effect of perfect and imperfect bonding on the postbuckling behaviour of the nanocomposite plate, all other studies are performed for imperfectly bonded GS-reinforced nanocomposite plate. The uni-axial/bi-axial compressive loads, N and the maximum transverse deflection is normalized as:

$$(8.2) \quad \lambda = \frac{Nb^2}{E_m h^3},$$

where E_m represents the elastic modulus of the matrix material.

The effect of type of bonding (i.e., perfect and imperfect) between GS and the matrix on the postbuckling response of SSSS GS-reinforced nanocomposite plate subjected to uni-axial compressive load is studied and also compared with that of the CNT-reinforced nanocomposite plate as shown in Fig. 10. It can be seen from Fig. 10 that the nanocomposite plate having perfect bonding between GS and the matrix material has the higher buckling load and postbuckling strength corresponding to a particular value of transverse deflection than imperfectly bonded GS reinforced PE nanocomposite plate. For instance, the perfectly bonded GS-reinforced nanocomposite plate has approximately 24.24% and 20.03% more buckling load and postbuckling strength (corresponding to $W^* = 0.5$), respectively than the imperfectly bonded GS-reinforced nanocomposite plate. This reduced enhancement in the buckling strength and postbuckling load can be attributed to the reduced enhancement in stiffness properties of the GS-nanocomposite as given in Table 8. GS-reinforced nanocomposite plate offers better buckling load and postbuckling strength than that of CNT reinforced nanocomposite plates regardless of the nature of bonding (i.e., perfect or imperfect). For instance, imperfectly bonded GS-reinforced nanocomposite plate has approximately 11.86% and 13.88% more buckling load and postbuckling strength (corresponding to $W^* = 0.5$), respectively than the imperfectly bonded CNT-reinforced nanocomposite plate. This reduction in the buckling strength and postbuckling load of CNT-reinforced nanocomposite plate can be attributed to

the reduced area of CNT available to load transfer from matrix materials as compared to GS-reinforced nanocomposite for the same volume fraction because of cylindrical and plate like the structure of CNT and GS respectively. GSs are found to be better reinforcements as also reported by [55].

Under uni-axial compression, the effect of GS-alignment in the direction of loading on the buckling load and postbuckling response of the GS-reinforced nanocomposite plate is studied, and the results are demonstrated in Fig. 11.

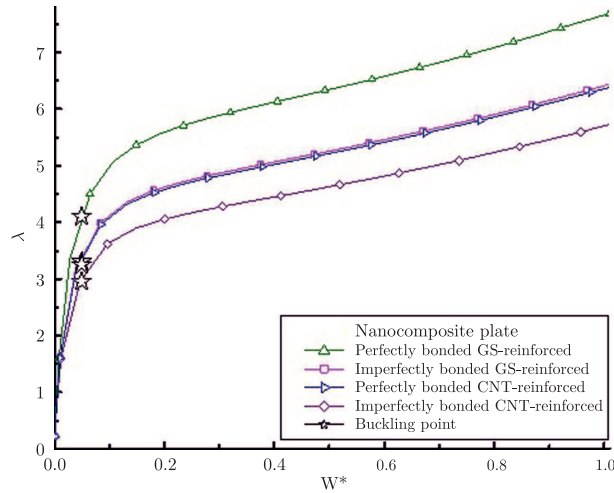


FIG. 10. Comparison of buckling and postbuckling behaviour of SSSS 3%-GS-reinforced PE nanocomposite plate subjected to uni-axial loading conditions.

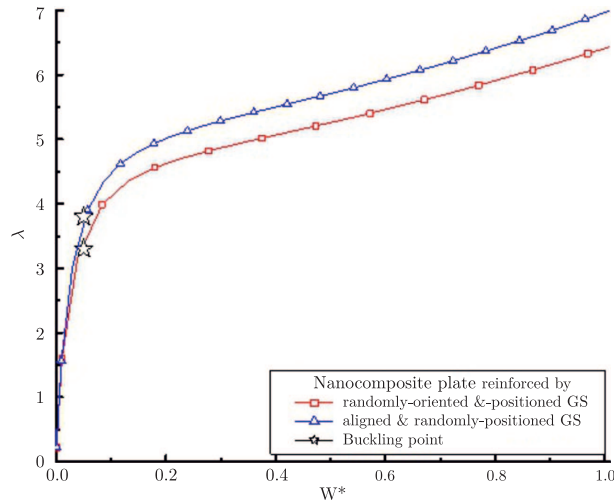


FIG. 11. Effect of alignment of GS on the buckling and postbuckling behaviour of SSSS GS-reinforced PE nanocomposite plate subjected to uni-axial loading conditions.

It can be observed from the Fig. 11 that the GS-alignment have the substantial effect on the buckling load and postbuckling response of the GS-reinforced PE nanocomposite plate than randomly-oriented and -positioned GS-reinforced nanocomposite plate. This finding can be explained by the fact that the aligned GS-reinforced nanocomposite possesses higher axial modulus (i.e., E_x) than uniformly-oriented and -positioned nanocomposite plates; therefore, offers better resistance to in-plane compressive loading. For instance, the imperfectly bonded aligned GS-reinforced nanocomposite plate has approximately 15.15% and 8.57% more buckling load and postbuckling strength (corresponding to $W^* = 0.5$), respectively than uniformly-oriented and -positioned imperfectly bonded GS-reinforced nanocomposite plate. Thus, higher buckling load and postbuckling strength are obtained for the GS nanocomposite plates reinforced with aligned GSs.

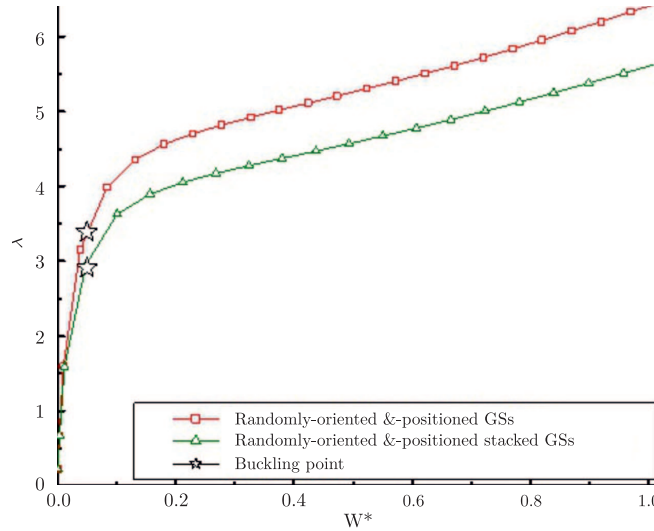


FIG. 12. Effect of stacking of GSs on the buckling and postbuckling behaviour of SSSS GS-reinforced PE nanocomposite plate subjected to uni-axial loading conditions.

Figures 12 and 13 represent the effect of agglomeration and length of GSs on the buckling load and postbuckling response of nanocomposite plates respectively. It is observed that, by stacking 3 GSs together, the percentage decrease in the buckling load and postbuckling strength (corresponding to $W^* = 0.5$) of the nanocomposite plate are 14.16 and 13.31%, respectively. On the other hand, in order to study the effect of length on the postbuckling behaviour of the nanocomposite plate, the length of GSs is shortened from 100 nm to 50 nm. The buckling load and postbuckling strength (corresponding to $W^* = 0.5$) of the nanocomposite plate are reduced by 5.01 and 4.57% respectively, by shortening the length of GSs to half.

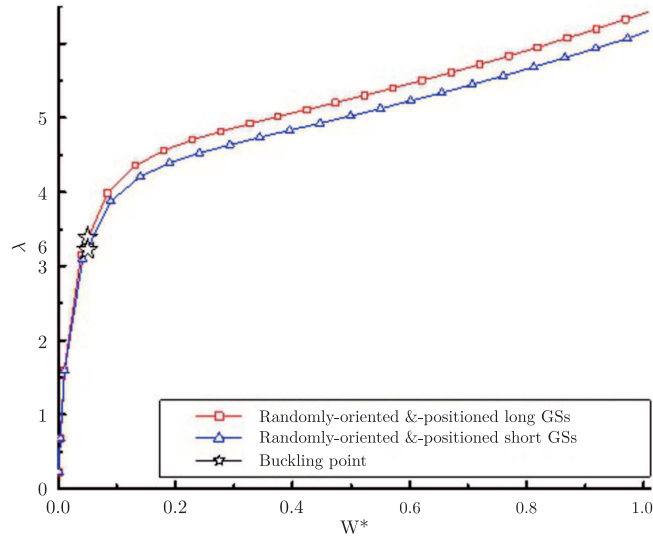


FIG. 13. Effect of length of GSs on the buckling and postbuckling behaviour of SSSS GS-reinforced PE nanocomposite plate subjected to uni-axial loading conditions.

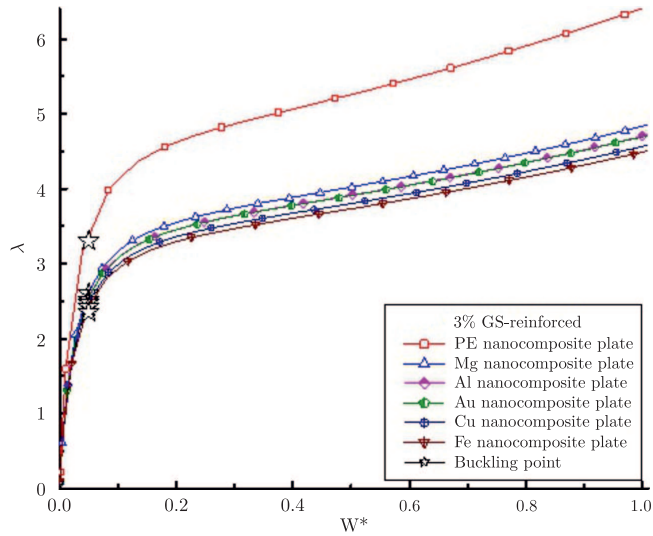


FIG. 14. Effect of matrix materials on buckling and postbuckling behaviour of SSSS nanocomposite plates with 3% volume fraction of GS.

The effects of matrix materials on buckling and postbuckling behaviour of SSSS nanocomposite plate with 3% volume fraction of GS are shown in Fig. 14. It can be seen from Fig. 14 that the GS reinforcement enhances the buckling load and postbuckling strength of nanocomposite plates made of soft materials more significantly than made of stiff materials. For example, 3% of GS reinforce-

ment increases the buckling load and postbuckling strength (corresponding to $W^* = 0.5$) of GS-PE nanocomposite by 40.4% and 41.5%, respectively, as compared to the corresponding values for pure matrix material (as given in Table 9); on the other hand, for GS-Fe nanocomposite, these values are limited to only 0.9% and 2.5%, respectively. This finding signifies the fact that GSs are far better reinforcing elements in polymer than stiff metals.

Table 9. Normalized buckling load and postbuckling strength (corresponding to $W^* = 5$) of different plates.

Matrix material	Normalized buckling load (i.e., λ_{cr})	Normalized postbuckling strength corresponding to $W^* = 0.5$ (i.e., λ)
Polyethylene (PE)	3.30	5.25
Magnesium (Mg)	2.60	4.02
Aluminum (Al)	2.52	3.91
Gold (Au)	2.48	3.90
Copper (Cu)	2.42	3.81
Iron (Fe)	2.35	3.72

The effects of geometric parameters (i.e., aspect and width-to-thickness ratios) on the buckling and postbuckling behaviour of the GS-reinforced nanocomposite plate are shown in Fig. 15 and Table 10, respectively. The results are obtained for imperfectly bonded GS-reinforced PE nanocomposite plate.

It is observed from Fig. 15, that with the increase in the aspect ratio (b_1/b_2) of nanocomposite plate, (where b_1 is the width of the plate in the x -direction,

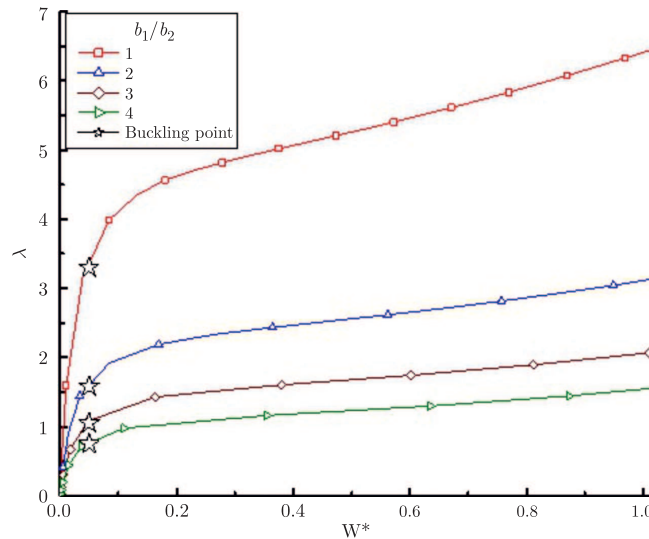


FIG. 15. Effect of aspect ratio (b_1/b_2) on the postbuckling response of SSSS imperfectly bonded GS-reinforced PE nanocomposite plate.

similarly b_2 represents the width of the plate in the y -direction) the buckling load and postbuckling strength of the nanocomposite plate decreases. The difference in the buckling load and postbuckling strength of GS nanocomposite plates of lower aspect ratios is substantial, and this difference decreases for the higher aspect ratio, as shown in Fig. 15. Therefore, the GS nanocomposite plates having higher aspect ratios possess almost the same buckling load and postbuckling response, indicating that for the higher aspect ratio the nanocomposite plate behaves more or less as a column.

Table 10. Effect of b/h ratio on the buckling load and postbuckling strength of GS-reinforced PE nanocomposite plate.

b/h	Buckling load		Postbuckling strength at $W^* = 5$	
	Dimensional (N_x) [kN/mm]	Non-dimensional (λ)	Dimensional (N_x) [kN/mm]	Non-dimensional (λ)
25	189.4164	3.12	307.8017	5.07
50	25.0430	3.30	39.6894	5.25
100	3.2252	3.40	4.9991	5.27
200	0.4055	3.42	0.6261	5.28

The effect of the width-to-thickness ratio (i.e., b/h) on the buckling load and postbuckling strength (at $W^* = 5$) of the GS-reinforced nanocomposite plate are given in Table 10. It is evident from Table 10 that with the increase in thickness of the GS-reinforced nanocomposite plate, its buckling load, and postbuckling strength increase substantially.

9. Conclusion

In the current study, an equivalent solid fibre (ESF) containing GS and the corresponding interphase zone is modelled, and that are dispersed randomly into the matrix material by the Boolean based RSA technique to make a nanocomposite. The Young's modulus and thickness of the interphase zone are derived by using the cohesive zone model. The effective stiffness properties of GS-reinforced nanocomposite material are evaluated with the application of the finite element method (FEM)-based numerical homogenization technique. The obtained stiffness properties of the nanocomposite material are further utilized to model and study the buckling and postbuckling behaviour of the GS-reinforced nanocomposite plate, with and without considering the interphase effect, subjected to in-plane compressive loading. Different studies are performed to study the effects of perfect and imperfect bonding between GS/CNT and the matrix material, GS-alignment, GS-stacking, length of GS, matrix materials, geometric param-

eters (i.e., the aspect ratio and width-to-thickness ratio), boundary conditions and type of loading (i.e., uni-axial and bi-axial compression) on the postbuckling behaviour of the GS-reinforced nanocomposite plate. The following conclusions based on the studies conducted are drawn:

- Effect of interphase between GS and PE matrix results in the reduced buckling load and postbuckling strength of the GS-reinforced nanocomposite plate as compared to the perfectly bonded GS-reinforced nanocomposite plate.
- GS-reinforced nanocomposite plate offers better buckling load and postbuckling strength than that of CNT-reinforced nanocomposite plates regardless of the nature of bonding (i.e., perfect or imperfect).
- GS reinforcement enhances the buckling load and postbuckling strength of nanocomposite plates made of soft materials (like PE) more significantly than made of stiff materials (like Fe).
- Buckling load and postbuckling strength of GS-reinforced PE nanocomposite plate under uni-axial compression load are substantially improved when the GSs are aligned in the direction of loading than that of the nanocomposite plate having randomly-oriented and -positioned GSs.
- Stacking of GSs and GSs having smaller length offer reductions in stiffness properties of the nanocomposite material, which therefore reduces the buckling load and postbuckling strength of nanocomposite plate.
- GS-reinforced nanocomposite plates having high aspect ratios possess almost the same buckling load and postbuckling strength, thus indicating that such plates would behave more or less like a column possessing only marginal postbuckling strength beyond buckling.
- The increase in the thickness of the GS-reinforced nanocomposite plate results in substantial improvement in its buckling load and postbuckling strength.

Acknowledgements

The present research work is carried out by utilizing the computation research facilities at the Material Research Center (MRC), Malaviya National Institute of Technology (MNIT) Jaipur. The authors would like to kindly acknowledge the MRC, MNIT Jaipur.

References

1. A.K. GEIM, K.S. NOVOSELOV, *The rise of graphene*, Nature, **6**, 183–191, 2007.
2. P.R. WALLACE, *The band theory of graphite*, Physical Review, **71**, 622–634, 1947.

3. M.P. SHARMA, L.G. JOHNSON, J.W. MCCLURE, *Diamagnetism of graphite*, Physics Letters A, **44**, 445–446, 1973.
4. E. FRADKIN, *Critical behaviour of disordered degenerate semiconductors I. Models, symmetries, and formalism*, Physical Review B, **33**, 3257–3262, 1986.
5. K.S. NOVOSELOV, A.K. GEIM, S.V. MOROZOV, D. JIANG, Y. ZHANG, S.V. DUBONOS, I.V. GRIGORIEVA, A.A. FIRSOV, *Electric field effect in atomically thin carbon films*, Science, **306**, 666–669, 2004.
6. I. OVID'KO, *Mechanical properties of graphene*, Reviews on Advanced Materials Science, **34**, 1–11, 2013.
7. T. KUILLA, S. BHADRA, D. YAO, N.H. KIM, S. BOSE, J.H. LEE, *Recent advances in graphene based polymer composites*, Progress in Polymer Science, **35**, 1350–1375, 2010.
8. S. STANKOVICH, D.A. DIKIN, G.H.B. DOMMETT, K.M. KOHLHAAS, E.J. ZIMNEY, E.A. STACH, R.D. PINER, S.T. NGUYEN, R.S. RUOFF, *Graphene-based composite materials*, Nature, **442**, 282–286, 2006.
9. H. KIM, C.W. MACOSKO, *Processing-property relationships of polycarbonate/graphene composites*, Polymer, **50**, 3797–3809, 2009.
10. M. EL ACHABY, A. QAISS, *Processing and properties of polyethylene reinforced by graphene nanosheets and carbon nanotubes*, Materials & Design, **44**, 81–89, 2013.
11. S. BASHIRVAND, A. MONTAZERI, *New aspects on the metal reinforcement by carbon nanofillers: A molecular dynamics study*, Materials & Design, **91**, 306–313, 2016.
12. A. FERREIDOOON, S. ALEAGHAEI, I. TARAGHI, *Mechanical properties of hybrid graphene/TiO₂ (rutile) nanocomposite: A molecular dynamics simulation*, Computational Materials Science, **102**, 220–227, 2015.
13. A. MONTAZERI, H. RAFII-TABAR, *Multiscale modeling of graphene- and nanotube-based reinforced polymer nanocomposites*, Physics Letters A, **375**, 4034–4040, 2011.
14. G.I. GIANNOPOULOS, I.G. KALLIVOKAS, *Mechanical properties of graphene based nanocomposites incorporating a hybrid interphase*, Finite Elements in Analysis and Design, **90**, 31–40, 2014.
15. Y. CHANDRA, E.I. SAAVEDRA FLORES, F. SCARPA, S. ADHIKARI, *Buckling of hybrid nanocomposites with embedded graphene and carbon nanotubes*, Physica E: Low-Dimensional Systems and Nanostructures, **83**, 434–441, 2016.
16. A. HEMMASIZADEH, M. MAHZOON, E. HADI, R. KHANDAN, *A method for developing the equivalent continuum model of a single layer graphene sheet*, Thin Solid Films, **516**, 7636–7640, 2008.
17. S. KITIPORNCHAI, X.Q. HE, K.M. LIEW, *Continuum model for the vibration of multilayered graphene sheets*, Physical Review B – Condensed Matter and Materials Physics, **72**, 75443, 2005.
18. M.M. SHOKRIEH, R. RAFIEE, *Prediction of Young's modulus of graphene sheets and carbon nanotubes using nanoscale continuum mechanics approach*, Materials & Design, **31**, 790–795, 2010.
19. Y.J. LIU, X.L. CHEN, *Evaluations of the effective material properties of carbon nanotube-based composites using a nanoscale representative volume element*, Mechanics of Materials, **35**, 69–81, 2003.

20. U.A. JOSHI, S.C. SHARMA, S.P. HARSHA, *Effect of waviness on the mechanical properties of carbon nanotube based composites*, Physica E: Low-Dimensional Systems and Nanostructures, **43**, 1453–1460, 2011.
21. D. KUMAR, A. SRIVASTAVA, *Elastic properties of CNT- and graphene-reinforced nanocomposites using RVE*, Steel and Composite Structures, **21**, 1085–1103, 2016.
22. A. ANJOMSHOA, A.R. SHAHIDI, B. HASSANI, E. JOMEHZADEH, *Finite element buckling analysis of multi-layered graphene sheets on elastic substrate based on nonlocal elasticity theory*, Applied Mathematical Modelling, **38**, 5934–5955, 2014.
23. A. NADERI, A.R. SAIDI, *Nonlocal postbuckling analysis of graphene sheets in a nonlinear polymer medium*, International Journal of Engineering Science, **81**, 49–65, 2014.
24. A. PARASHAR, P. MERTINY, *Representative volume element to estimate buckling behavior of graphene/polymer nanocomposite*, Nanoscale Research Letters, **7**, 515, 2012.
25. P. JOSHI, S.H. UPADHYAY, *Analysis of alignment effect on carbon nanotube layer in nanocomposites*, Physica E: Low-Dimensional Systems and Nanostructures, **66**, 221–227, 2015.
26. S.K. GEORGANTZINOS, G.I. GIANNOPOULOS, N.K. ANIFANTIS, *Effective Young's modulus of carbon nanotube composites: From multi-scale finite element predictions to an analytical rule*, Journal of Computational and Theoretical Nanoscience, **7**, 1436–1442, 2010.
27. G.I. GIANNOPOULOS, S.K. GEORGANTZINOS, N.K. ANIFANTIS, *A semi-continuum finite element approach to evaluate the Young's modulus of single-walled carbon nanotube reinforced composites*, Composites Part B: Engineering, **41**, 594–601, 2010.
28. S.K. GEORGANTZINOS, G.I. GIANNOPOULOS, N.K. ANIFANTIS, *Investigation of stress-strain behavior of single walled carbon nanotube/rubber composites by a multi-scale finite element method*, Theoretical and Applied Fracture Mechanics, **52**, 158–164, 2009.
29. B. ARASH, Q. WANG, V.K. VARADAN, *Mechanical properties of carbon nanotube/polymer composites*, Scientific Reports, **4**, 6479, 2014.
30. L.Y. JIANG, Y. HUANG, H. JIANG, G. RAVICHANDRAN, H. GAO, K.C. HWANG, B. LIU, *A cohesive law for carbon nanotube/polymer interfaces based on the van der Waals force*, Journal of the Mechanics and Physics of Solids, **54**, 2436–2452, 2006.
31. J. ZHAO, J.W. JIANG, Y. JIA, W. GUO, T. RABCZUK, *A theoretical analysis of cohesive energy between carbon nanotubes, graphene and substrates*, Carbon, **57**, 108–119, 2013.
32. A. SRIVASTAVA, D. KUMAR, *A continuum model to study interphase effects on elastic properties of CNT/GS-nanocomposite*, Materials Research Express, **4**, 25036, 2017.
33. A. HERNÁNDEZ-PÉREZ, F. AVILÉS, *Modeling the influence of interphase on the elastic properties of carbon nanotube composites*, Computational Materials Science, **47**, 926–933, 2010.
34. M.M. SHOKRIEH, R. RAFIEE, *Prediction of mechanical properties of an embedded carbon nanotube in polymer matrix based on developing an equivalent long fiber*, Mechanics Research Communications, **37**, 235–240, 2010.
35. S. CHATTERJEE, F. NAFEZAREFI, N.H. TAI, L. SCHLAGENHAUF, F.A. NÜESCH, B.T.T. CHU, *Size and synergy effects of nanofiller hybrids including graphene nanoplatelets and carbon nanotubes in mechanical properties of epoxy composites*, Carbon, **50**, 5380–5386, 2012.

36. L.Y. CHEN, H. KONISHI, A. FEHRENBACHER, C. MA, J.Q. XU, H. CHOI, H.F. XU, F.E. PFEFFERKORN, X.C. LI, *Novel nanoprocessing route for bulk graphene nanoplatelets reinforced metal matrix nanocomposites*, *Scripta Materiala*, **67**, 29–32, 2012.
37. J. KIM, J. OH, K.Y. LEE, I. JUNG, M. PARK, *Dispersion of graphene-based nanocarbon fillers in polyamide 66 by dry processing and its effect on mechanical properties*, *Composites Part B: Engineering*, **114**, 445–456, 2017.
38. M. FANG, K. WANG, H. LU, Y. YANG, S. NUTT, *Covalent polymer functionalization of graphene nanosheets and mechanical properties of composites*, *Journal of Materials Chemistry*, **19**, 7098, 2009.
39. X. LIN, X. SHEN, Q. ZHENG, N. YOUSEFI, L. YE, Y.W. MAI, J.K. KIM, *Fabrication of highly-aligned, conductive, and strong graphene papers using ultralarge graphene oxide sheets*, *ACS Nano*, **6**, 10708–10719, 2012.
40. J. FEDER, *Random sequential adsorption*, *Journal of Theoretical Biology*, **87**, 2, 237–254, 1980.
41. S. KARI, H. BERGER, U. GABBERT, *Numerical evaluation of effective material properties of randomly distributed short cylindrical fibre composites*, *Computational Materials Science*, **39**, 198–204, 2007.
42. Y. PAN, L. IORGA, A.A. PELEGRI, *Analysis of 3D random chopped fiber reinforced composites using FEM and random sequential adsorption*, *Computational Materials Science*, **43**, 450–461, 2008.
43. M. BAILAKANAVAR, Y. LIU, J. FISH, Y. ZHENG, *Automated modeling of random inclusion composites*, *Engineering with Computers*, **30**, 609–625, 2012.
44. H. LIU, D. ZENG, Y. LI, L. JIANG, *Development of RVE-embedded solid elements model for predicting effective elastic constants of discontinuous fiber reinforced composites*, *Mechanics of Materials*, **93**, 109–123, 2016.
45. M. SONG, S. KITIPORNCHAI, J. YANG, *Free and forced vibrations of functionally graded polymer composite plates reinforced with graphene nanoplatelets*, *Composite Structures*, **159**, 579–588, 2017.
46. H. WU, J. YANG, S. KITIPORNCHAI, *Dynamic instability of functionally graded multilayer graphene nanocomposite beams in thermal environment*, *Composite Structures*, **162**, 244–254, 2017.
47. J. YANG, H. WU, S. KITIPORNCHAI, *Buckling and postbuckling of functionally graded multilayer graphene platelet-reinforced composite beams*, *Composite Structures*, **161**, 111–118, 2017.
48. H.S. SHEN, Y. XIANG, F. LIN, *Buckling and postbuckling of functionally graded graphene-reinforced composite laminated plates in thermal environments*, *Composites Part B*, **119**, 67–78, 2017.
49. A. SRIVASTAVA, D. KUMAR, *Post-buckling behaviour of carbon-nanotube-reinforced nanocomposite plate*, *Sādhanā*, **42**, 129–141, 2017.
50. J. FAN, *Multiscale Analysis of Deformation and Failure of Materials*, Wiley, New York, 2011.
51. A. WHITE, *Intermolecular potentials of mixed systems: Testing the Lorentz–Berthelot mixing rules with ab initio calculations*, Defence Science and Technology Organisation, DSTO-TN-0302, Melbourne, 2000.

52. D. BODA, D. HENDERSON, *The effects of deviations from Lorentz–Berthelot rules on the properties of a simple mixture*, Molecular Physics. An International Journal Interface Between Chemistry Physics, **106**, 2367–2370, 2008.
53. A.K. KAW, *Mechanics of Composite Materials*, CRC Press Taylor & Francis Group, London, New York, 2006.
54. A. SRIVASTAVA, D. KUMAR, *Postbuckling of nanocomposite plate reinforced with randomly oriented and dispersed CNTs modeled through RSA technique*, International Journal for Multiscale Computational Engineering, **14**, 585–606, 2016.
55. M.A. RAFIEE, J. RAFIEE, Z. WANG, H. SONG, Z. YU, N. KORATKAR, *Enhanced mechanical properties of nanocomposites at low graphene content*, ACS Nano, **3**, 3884–3890, 2009.
56. T. KUBIAK, *Static and Dynamic Buckling of Thin-Walled Plate Structures*, Springer International Publishing, Switzerland, 2013.
57. B.W.R. FORDE, S.F. STIEMER, *Improved arc length orthogonality methods for nonlinear finite element analysis*, Computers & Structures, **27**, 625–630, 1987.
58. A. SRIVASTAVA, D. KUMAR, *Mechanical characterization and postbuckling behavior of carbon nanotube-carbon fiber reinforced nanocomposite laminate*, Proceedings of the Institution of Mechanical Engineers. Part C Journal of Mechanical Engineering Science, **232**, 106–123, 2016.
59. V. MITTAL, S. KIM, S. NEUHOFER, C. PAULIK, *Polyethylene/graphene nanocomposites: effect of molecular weight on mechanical, thermal, rheological and morphological properties*, Colloid and Polymer Science, **294**, 691–704, 2016.
60. M. RASHAD, F. PAN, A. TANG, M. ASIF, J. SHE, J. GOU, J. MAO, H. HU, *Development of magnesium-graphene nanoplatelets composite*, Journal of Composite Materials, **49**, 285–293, 2015.
61. D. LIN, C.R. LIU, G.J. CHENG, *Single-layer graphene oxide reinforced metal matrix composites by laser sintering: Microstructure and mechanical property enhancement*, Acta Materialia, **80**, 183–193, 2014.
62. C. ZHAO, J. WANG, *Fabrication and Tensile properties of graphene/copper composites prepared by electroless plating for structural applications*, Physica Status Solidi A, Applications and Materials Science, **211**, 2878–2885, 2014.
63. S.J. NITEESH KUMAR, R. KESHAVAMURTHY, M.R. HASEEBUDDIN, P.G. KOPPAD, *Mechanical properties of aluminium-graphene composite synthesized by powder metallurgy and hot extrusion*, Transactions of the Indian Institute of Metals, **70**, 605–613, 2017.
64. S.K. CHIEN, Y.T. YANG, C.K. CHEN, *A molecular dynamics study of the mechanical properties of graphene nanoribbon-embedded gold composites*, Nanoscale, **3**, 4307, 2011.
65. S. PLIMPTON, *Fast parallel algorithms for short-range molecular dynamics*, Journal of Computational Physics, **117**, 1–19, 1995.
66. B. WENXING, Z. CHANGCHUN, C. WANZHAO, *Simulation of Young’s modulus of single-walled carbon nanotubes by molecular dynamics*, Physica B: Condensed Matter, **352**, 156–163, 2004.
67. K. ALZEBDEH, *Evaluation of the in-plane effective elastic moduli of single-layered graphene sheet*, International Journal of Mechanics and Materials Design, **8**, 269–278, 2012.

68. X.L. CHEN, Y.J. LIU, *Square representative volume elements for evaluating the effective material properties of carbon nanotube-based composites*, Computational Materials Science, **29**, 1–11, 2004.
69. P. JOSHI, S.H. UPADHYAY, *Evaluation of elastic properties of multi walled carbon nanotube reinforced composite*, Computational Materials Science, **81**, 332–338, 2014.
70. P. SUNDARESAN, G. SINGH, G. VENKATESWARA RAO, *Buckling and post-buckling analysis of moderately thick laminated rectangular plates*, Computers & Structures, **61**, 79–86, 1996.
71. T. LE-MANH, J. LEE, *Postbuckling of laminated composite plates using NURBS-based isogeometric analysis*, Composite Structures, **109**, 286–293, 2014.

Received September 11, 2017; revised version December 28, 2017.
